*Progress In Electromagnetics Research, PIER 67, 205–230, 2007*

# APPLICATION OF MODE MATCHING METHOD TO ANALYSIS OF AXISYMMETRIC COAXIAL DISCONTINUITY STRUCTURES USED IN PERMEABILITY AND/OR PERMITTIVITY MEASUREMENT

**R. F. Huang and D. M. Zhang**

School of Electrical and Electronic Engineering
Nanyang Technological University
Singapore

**Abstract**—This paper presents a mode matching method to analyze axisymmetric coaxial discontinuity structures, commonly used in the permeability and/or permittivity measurement. By performing the mode matching procedures at all discontinuity interfaces, a set of general simultaneous equations are derived, which can be easily solved. The $s$ parameters and field distribution in the structures are readily obtained from the solution to the simultaneous equations. As a preliminary preparation for the mode matching method, the propagation constants of all the sections in the structure have to be solved. A one-dimensional frequency domain finite difference method is presented in this paper to efficiently solve the propagation constants for the multi-layered axisymmetric structures. Numerical examples show that the results obtained from the method in this paper are in good agreement with those from other methods in the published literature papers, and the method presented here has much higher efficiency.

## 1. INTRODUCTION

COAXIAL discontinuity structures are widely used as an element of microwave devices, and commonly used in the permeability and/or permittivity measurement for materials [1–6]. This kind of structures are usually analyzed in the frequency domain by using mode matching method [3, 4, 7, 8], full-wave spectral-domain method [9], finite element method [5, 10], or frequency domain transmission line matrix method [6], or in the time domain by using FDTD method [11–14]. Although the numerical methods such as finite element method and FDTD can

deal with complex irregular structures with more flexibility, for the structures considered in this paper, it can be expected that the mode matching method has more advantages since it conforms closely to physical reality [7] and apparently has much less unknown variables. For some specific axisymmetrical coaxial discontinuity structures, mode matching method has been successfully applied [3, 4, 8]. It is the purpose of this paper to present a general approach based on the mode matching method to deal with this kind of coaxial discontinuity structures. As we will see in Section 4, the electromagnetic waves in this kind of discontinuity structures can be described by a set of rather simple simultaneous equations which can be easily solved.

Since the mode matching method is based on the modal expansion of the total field, the propagation constants of the modal fields in the structure have to be solved first. Usually, propagation constants of waveguides or transmission lines are solved by analytical/semi-analytical method for simple structures or by numerical methods such as finite difference method [15–19] and finite element method [20, 21] for complex structures. It is worthwhile to mention that in [15] a compact two-dimensional frequency domain finite difference method is presented to solve the propagation constants of a general waveguide. In that method the longitudinal field components are eliminated and only four transverse field components are involved in the final resulting eigen equation. In [16] and [17], the compact two-dimensional frequency domain finite difference method is further improved with the resultant eigenvalue problem involving only two field components.

In this paper, for the uniformly filled coaxial and circular waveguides, the propagation constants are solved by existent semi-analytical methods. For the multi-layer filled axisymmetric coaxial and circular waveguides, a one-dimensional frequency domain finite difference method is presented to efficiently solve the propagation constants. In the one-dimensional frequency domain finite difference method, with the axisymmetric geometry of the considered structures taken into account, the resultant eigenvalue problem involves only one field component. Thus it considerably reduces the required CPU time. For the multi-layered axisymmetric coaxial waveguides, a semi-analytical approach, the field matching technique, is presented in [22] to solve the propagation constants. Since such a method has to search the propagation constants in the complex plane by numerical routines at small step widths, as is described in detail in Section 5, by comparison the one-dimensional frequency domain finite difference method in this paper has much higher efficiency.

The organization of the paper is as follows. The propagation constants of the axisymmetric structures under consideration are

solved in Section 2. Based on the solutions of the propagation constants, in Section 3, the corresponding modal field patterns are determined. In Section 4, a set of general formulae which describe the matching conditions of the waves at the interfaces in the structures are derived. Several numerical examples are given in Section 5 to verify the methods in this paper. Finally, a brief conclusion is drawn in Section 6.

## 2. SOLVING PROPAGATION CONSTANTS IN AXISYMMETRICAL STRUCTURES

In this paper, among the high order modes, we are only interested in the dispersion characteristics of symmetrical TM modes, i.e., those with axial symmetry, which are the only high order modes excited in axisymmetrical discontinuity structures under TEM wave excitation.

For the uniformly filled coaxial waveguides, the propagation constant $\gamma$ of the TEM mode can be expressed as [23]:

$$\gamma = j\omega\sqrt{\mu\varepsilon}, \tag{1}$$

where $\mu$ and $\varepsilon$ are the permeability and the permittivity of the filling material respectively. The propagation constants $\gamma$ of the symmetrical TM modes satisfy the following equation [23]:

$$J_0(a)N_0(ak) - N_0(a)J_0(ak) = 0, \tag{2}$$

where

$$a = k_c R_1 \tag{3}$$

$$k = R_2/R_1 \tag{4}$$

$$k_c = \sqrt{\omega^2\mu\varepsilon + \gamma^2}. \tag{5}$$

Since the roots of (2), i.e., $a$, are all real numbers, they can be easily searched by numerical methods. Thus $\gamma$ can be solved without much difficulty.

For the uniformly filled circular waveguide, the propagation constants $\gamma$ of the symmetrical TM modes are solved from the roots of the following equation [23]:

$$J_0(b) = 0, \tag{6}$$

where

$$b = k_c R_2, \tag{7}$$

and $k_c$ is defined in (5). Again, since the roots of (6), i.e., $b$, are all real numbers, $\gamma$ can be easily solved.

For the multi-layered coaxial or circular waveguides, solving the propagation constants is not as easy as for the uniformly filled counterparts. A one-dimensional frequency domain finite difference method is presented below to efficiently solve the propagation constants of this kind of structures. Without loss of generality, an axisymmetrical structure shown in Fig. 1 is considered. The inner and the outer conductors are assumed to be perfect electric ones. Without the inner conductor, the structure becomes a circular waveguide.

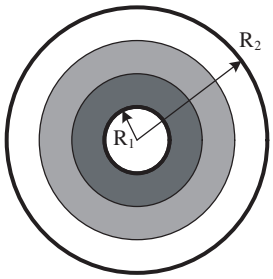


**Figure 1.** Cross section of a multi-layer filled axisymmetric structure.

Based on Maxwell's curl equations in the cylindrical coordinates, the following equations governing the field components of TM modes can be obtained [24]:

$$\frac{\partial E_r}{\partial z} - \frac{\partial E_z}{\partial r} = -j\omega\mu H_\phi, \tag{8}$$

$$-\frac{\partial H_\phi}{\partial z} = j\omega\varepsilon E_r, \tag{9}$$

$$\frac{1}{r}\frac{\partial}{\partial r}(rH_\phi) = j\omega\varepsilon E_z \tag{10}$$

Since in the problem of dispersion characteristics analysis, the structure is considered to be uniform along the $z$ axis, (8) and (9) can be rewritten as follows:

$$-\gamma E_r - \frac{\partial E_z}{\partial r} = -j\omega\mu H_\phi, \tag{11}$$

$$E_r = \frac{\gamma}{j\omega\varepsilon} H_\phi, \tag{12}$$

where $\gamma$ is the propagation constant to be solved.

Eliminating the $E_r$ components in the two equations above by substituting (12) into (11) results in the following equation:

$$\left(\omega^2\mu\varepsilon + \gamma^2\right) H_\phi + j\omega\varepsilon\frac{\partial E_z}{\partial r} = 0. \tag{13}$$

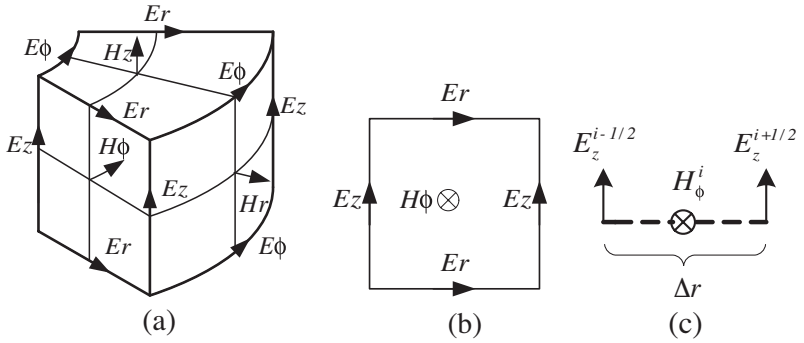


**Figure 2.** Finite difference cells in different dimensions in cylindrical coordinates. (a) three-dimensional finite difference cell. (b) two-dimensional TM mode finite difference cell. (c) one-dimensional TM mode finite difference cell.

In the finite difference method, finite difference cells are used to discretize the differential equations. The conventional three-dimensional finite difference cell in cylindrical coordinate is shown in Fig. 2(a). Since the field components are independent of the azimuthal angle $\phi$, the two-dimensional finite difference cell for TM modes in Fig. 2(b) can be obtained by projecting the three-dimensional finite difference cell onto $r$-$z$ plane and neglecting the field components of TE modes. For the differential Equation (13), since the $E_r$ components are eliminated, one-dimensional finite difference cell in Fig. 2(c), which originates from neglecting the $E_r$ components in the two-dimensional finite difference cell, can be simply used to discretize the equation as below:

$$\left(\omega^2\mu_i\varepsilon_i + \gamma^2\right) H_\phi^i + j\omega\varepsilon_i \frac{E_z^{i+1/2} - E_z^{i-1/2}}{\Delta r} = 0, \tag{14}$$

where $\mu_i$ and $\varepsilon_i$ are the complex permeability and permittivity of cell $(i)$ respectively. For simplicity, we assume that all the cells have the same width of $\Delta r$.

Discretizing (10) by using the one-dimensional finite difference cell we then get

$$j\omega\varepsilon_i \frac{E_z^{i+1/2}}{\Delta r} = \frac{\varepsilon_i \left(r_{i+1} H_\phi^{i+1} - r_i H_\phi^i\right)}{\varepsilon_{i+1/2} r_{i+1/2} \Delta r^2}, \tag{15}$$

$$-j\omega\varepsilon_i \frac{E_z^{i-1/2}}{\Delta r} = \frac{\varepsilon_i \left(r_{i-1} H_\phi^{i-1} - r_i H_\phi^i\right)}{\varepsilon_{i-1/2} r_{i-1/2} \Delta r^2}, \tag{16}$$

where $r_{i+1/2}$ is the distance between the center of cell $(i)$ and the axis of the structure, and $\varepsilon_{i+1/2}$ the complex permittivity at the interface between cell $(i)$ and cell $(i+1)$, which can be calculated as below by employing spatial average [12–16].

$$\varepsilon_{i+1/2} = \frac{\varepsilon_i + \varepsilon_{i+1}}{2} \tag{17}$$

Equation (16) is derived from (15) if we set $i = i - 1$. The $E_z$ components at the surface of perfect electric conductor are set to zero in (14) as the boundary conditions.

For the circular waveguides without the inner conductor in Fig. 1, Equation (16) cannot be used to evaluate $E_z$ at $r = 0$, since there is no cell to the left of the axis in the computation area. To evaluate this component, the integral form of Maxwell's Equation [24] as shown below is used:

$$\oint \mathbf{H} d\mathbf{I} = j\omega \int_s \varepsilon \mathbf{E} d\mathbf{S}. \tag{18}$$

From (18), $E_z$ at $r = 0$ can be expressed as:

$$-j\omega\varepsilon_i \frac{E_z^{i-1/2}}{\Delta r} = \frac{-4H_\phi^i}{\Delta r^2}, \qquad i = 1. \tag{19}$$

Eliminating the $E_z$ components by substituting (15), (16) and (19) into (14) and implementing the boundary conditions results in the standard eigenvalue problem:

$$[A][H_\phi] = \gamma^2 [H_\phi], \tag{20}$$

where $[A]$ is a sparse and banded matrix.

Solving the eigenvalue problem we can obtain the propagation constants and the corresponding magnetic field distribution in the $r$ direction, i.e., the eigenvectors, which can be used to determine the modal field patterns in the following section. Since the eigenvalue problem (20) is only related to $H_\phi$, it can be seen that the propagation constant of the quasi-TEM mode is also included in the solution.

## 3. DETERMINATION THE MODAL FIELD PATTERNS

For the TEM mode in the uniformly filled coaxial waveguides, the field components $E_r$ and $H_\phi$ can be expressed as below [3, 4]:

$$E_r = \frac{C^1}{r} e^{-\gamma z}, \tag{21}$$

$$H_\phi = \sqrt{\frac{\varepsilon}{\mu}} \frac{C^1}{r} e^{-\gamma z}, \tag{22}$$

where $C^1$ denotes a constant.

For the TM or the quasi-TEM modes, from Maxwell's equations in the cylindrical coordinates, the equation governing $E_z$ can be written as [24]:

$$\left[\frac{1}{r}\frac{\partial}{\partial r}\left(r\frac{\partial}{\partial r}\right)+\frac{1}{r^2}\frac{\partial^2}{\partial\phi^2}+k_c^2\right]E_z=0, \tag{23}$$

where

$$k_c^2=\omega^2\mu\varepsilon+\gamma^2. \tag{24}$$

Based on the assumption that the field components are independent of the azimuthal angle $\Phi$, the solution of (23) can be expressed as [25]:

$$E_z=\frac{k_c^x}{\gamma}\left[C^xJ_0\left(k_c^xr\right)+D^xN_0\left(k_c^xr\right)\right]e^{-\gamma z}, \tag{25}$$

where the superscript $x$ is the layer number ($x=1,2,\cdots$).

The transverse field components $E_r$ and $H_\phi$ can be expressed in terms of the field components $E_z$ and $H_z$ as follows [24]:

$$E_r = -\frac{1}{k_c^2}\left[\gamma\frac{\partial E_z}{\partial r}+\frac{j\omega\mu}{r}\frac{\partial H_z}{\partial\phi}\right], \tag{26}$$

$$H_\phi = -\frac{1}{k_c^2}\left[\frac{\gamma}{r}\frac{\partial H_z}{\partial\phi}+j\omega\varepsilon\frac{\partial E_z}{\partial r}\right]. \tag{27}$$

Substituting (25) into (26) and (27), and ignoring magnetic field component $H_z$ of the TE modes, we can obtain:

$$E_r = \left[C^xJ_1\left(k_c^xr\right)+D^xN_1\left(k_c^xr\right)\right]e^{-\gamma z}, \tag{28}$$

$$H_\phi = \frac{j\omega\varepsilon^x}{\gamma}\left[C^xJ_1\left(k_c^xr\right)+D^xN_1\left(k_c^xr\right)\right]e^{-\gamma z}. \tag{29}$$

For the uniformly filled coaxial waveguides, since $E_z|_{r=R_1}=0$ and $E_z|_{r=R_2}=0$, from (25), the coefficient $D^1$ in (25), (28) and (29) can be expressed as:

$$D^1=-\frac{J_0\left(k_cR_1\right)}{N_0\left(k_cR_1\right)}C^1=-\frac{J_0\left(k_cR_2\right)}{N_0\left(k_cR_2\right)}C^1. \tag{30}$$

For the uniformly filled circular waveguides, since $E_z|_{r=0}\neq\infty$, from (25), the coefficient $D^1$ in (25), (28) and (29) is zero.

For the multi-layered coaxial and circular waveguides, as mentioned in the last section, the magnetic field distribution along the $r$ direction corresponding to the propagation constants can be solved as the eigenvectors of (20). Thus from (29), $C^x$ and $D^x$ can be solved by using the least square method.

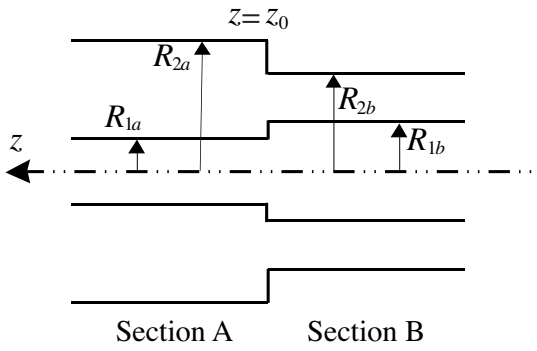


**Figure 3.** Axisymmetrical discontinuity under consideration.

## 4. MODE MATCHING METHOD FOR AXISYMMETRICAL COAXIAL DISCONTINUITY STRUCTURES

For the general axisymmetrical structure discontinuity shown in Fig. 3, both sections may have multiple layers of filling materials. Also both sections may not necessarily have the inner conductors. A coaxial discontinuity structure may have many such discontinuities. Naturally, the first section of the structure, to which the source is connected, must have the inner conductor to support TEM wave excitation.

From (21), (22), (28) and (29), the transverse electromagnetic field components of the two sections can be written as follows:

$$E_{Ar} = 0, \qquad 0 < r < R_{1a}, \tag{31}$$

$$E_{Ar} = \frac{A_0}{r}\left[e^{\gamma_{A0}(z-z_0)} + \Gamma_{A0}e^{-\gamma_{A0}(z-z_0)}\right] + \sum_{i=1}^{\infty} A_i Z_{A1}\left(k_{ci}^x r\right) \left[e^{\gamma_i(z-z_0)} + \Gamma_{Ai}e^{-\gamma_i(z-z_0)}\right], \qquad R_{1a} < r < R_{2a}, \tag{32}$$

$$H_{A\phi} = 0, \qquad 0 < r < R_{1a}, \tag{33}$$

$$H_{A\phi} = -\sqrt{\frac{\varepsilon_A}{\mu_A}}\frac{A_0}{r}\left[e^{\gamma_{A0}(z-z_0)} - \Gamma_{A0}e^{-\gamma_{A0}(z-z_0)}\right] + \sum_{i=1}^{\infty}\frac{-j\omega\varepsilon^x}{\gamma_i}A_i Z_{A1}\left(k_{ci}^x r\right)\left[e^{\gamma_i(z-z_0)} - \Gamma_{Ai}e^{-\gamma_i(z-z_0)}\right], \quad R_{1a} < r < R_{2a}, \tag{34}$$

$$E_{Br} = 0, \qquad 0 < r < R_{1b}, \tag{35}$$

$$E_{Br} = \frac{B_0}{r}\left[e^{\gamma_{B0}(z-z_0+d)} + \Gamma_{B0}e^{-\gamma_{B0}(z-z_0+d)}\right] + \sum_{m=1}^{\infty} B_m Z_{B1}\left(k_{cm}^y r\right) \left[e^{\gamma_m(z-z_0+d)} + \Gamma_{Bm}e^{-\gamma_m(z-z_0+d)}\right], \quad R_{1b} < r < R_{2b}, \tag{36}$$

$$H_{B\phi} = 0, \quad 0 < r < R_{1b}, \tag{37}$$

$$H_{B\phi} = -\sqrt{\frac{\varepsilon_B}{\mu_B}}\frac{B_0}{r}\left[e^{\gamma_{B0}(z-z_0+d)} - \Gamma_{B0}e^{-\gamma_{B0}(z-z_0+d)}\right] + \sum_{m=1}^{\infty} \frac{-j\omega\varepsilon^y}{\gamma_m} B_m Z_{B1}\left(k_{cm}^y r\right)\left[e^{\gamma_m(z-z_0+d)} - \Gamma_{Bm}e^{-\gamma_m(z-z_0+d)}\right] \quad R_{1b} < r < R_{2b}, \tag{38}$$

where $d$ is the length of Section B, $\gamma_{A0}$ is the propagation constant of the TEM mode in Section A when Section A is a uniformly filled coaxial waveguide with the permeability and the permittivity of the filling material being $\mu_A$ and $\varepsilon_A$ respectively, $A_0$ is zero except the case that Section A is a uniformly filled coaxial waveguide, $\gamma_{B0}$, $B_0$, $\mu_B$ and $\varepsilon_B$ in Section B are the counterparts of $\gamma_{A0}$, $A_0$, $\mu_0$ and $\varepsilon_A$ respectively, and

$$Z_{An}\left(k_{ci}^x r\right) = \left[C_i^x J_n\left(k_{ci}^x r\right) + D_i^x N_n\left(k_{ci}^x r\right)\right], \tag{39}$$

$$Z_{Bn}\left(k_{cm}^y r\right) = \left[C_m^y J_n\left(k_{cm}^y r\right) + D_m^y\left(k_{cm}^x r\right)\right]. \tag{40}$$

The continuity of the transverse electromagnetic field components at the discontinuity interface provides the following equations:

$$E_{Ar}|_{z=z_0} = E_{Br}|_{z=z_0}, \ (\min(R_{1a}, R_{1b}) < r < \max(R_{2a}, R_{2b})), \tag{41}$$

$$H_{A\phi}|_{z=z_0} = H_{B\phi}|_{z=z_0}, \ (\max(R_{1a}, R_{1b}) < r < \min(R_{2a}, R_{2b})). \tag{42}$$

The following orthogonality relation between different modes in Section A or B holds [7]:

$$\int_{R_1}^{R_2} (\mathbf{E}_p \times \mathbf{H}_q) \cdot \mathbf{u_z} 2\pi r dr = 0, \tag{43}$$

where $R_2$ is the inner radius of the outer conductor, $R_1$ is the outer radius of the inner conductor, and $p \neq q$. In the case there is no inner conductor, $R_1$ is zero.

The first step of the mode matching procedure is to perform the following integral at both sides of (41):

$$\int_{R_{1a}}^{R_{2a}} E_{Ar} H_{A\phi i} 2\pi r dr. \tag{44}$$

By making use of the orthogonality relation (43), together with the Lommel integrals, the following equations can be obtained:

$$
\begin{aligned}
A_0(1+\Gamma_{A0})\int_{R_{1a}}^{R_{2a}}\frac{1}{r}dr &= A_0(1+\Gamma_{A0})\ln\frac{R_{2a}}{R_{1a}} \\
&= B_0\left(e^{\gamma_{B0}d}+\Gamma_{B0}e^{-\gamma_{B0}d}\right)\int_{\max(R_{1a},R_{1b})}^{\min(R_{2a},R_{2b})}\frac{1}{r}dr \\
&\quad+\sum_{m=1}^{\infty}B_m\left(e^{\gamma_m d}+\Gamma_{Bm}e^{-\gamma_m d}\right)\int_{\max(R_{1a},R_{1b})}^{\min(R_{2a},R_{2b})}Z_{B1}(k_{cm}^{y}r)dr \\
&= B_0\left(e^{\gamma_{B0}d}+\Gamma_{B0}e^{-\gamma_{B0}d}\right)\ln\frac{\min(R_{2a},R_{2b})}{\max(R_{1a},R_{1b})} \\
&\quad+\sum_{m=1}^{\infty}B_m\left(e^{\gamma_m d}+\Gamma_{Bm}e^{-\gamma_m d}\right)\sum_{y=y_1}^{y_t}\int_{R_{1y}}^{R_{2y}}Z_{B1}(k_{cm}^{y}r)dr \\
&= B_0\left(e^{\gamma_{B0}d}+\Gamma_{B0}e^{-\gamma_{B0}d}\right)\ln\frac{\min(R_{2a},R_{2b})}{\max(R_{1a},R_{1b})} \\
&\quad+\sum_{m=1}^{\infty}B_m\left(e^{\gamma_m d}+\Gamma_{Bm}e^{-\gamma_m d}\right) \\
&\quad\times\sum_{y=y_1}^{y_t}\left[-Z_{B0}(k_{cm}^{y}R_{2y})+Z_{B0}(k_{cm}^{y}R_{1y})\right]/k_{cm}^{y}, \qquad (45)
\end{aligned}
$$

$$
\begin{aligned}
A_i(1+\Gamma_{Ai})&\int_{R_{1a}}^{R_{2a}}\varepsilon^x Z_{A1}^2(k_{ci}^{x}r)rdr \\
&= A_i(1+\Gamma_{Ai})\sum_{x=1}^{t_A}\varepsilon^x\left[f_{Ai}^{x}(R_{2x})-f_{Ai}^{x}(R_{1x})\right] \\
&= B_0\left[e^{\gamma_{B0}d}+\Gamma_{B0}e^{-\gamma_{B0}d}\right]\int_{\max(R_{1a},R_{1b})}^{\min(R_{2a},R_{2b})}\varepsilon^x Z_{A1}(k_{ci}^{x}r)dr \\
&\quad+\sum_{m=1}^{\infty}B_m\left[e^{\gamma_m d}+\Gamma_{Bm}e^{-\gamma_m d}\right] \\
&\quad\times\int_{\max(R_{1a},R_{1b})}^{\min(R_{2a},R_{2b})}\varepsilon^x Z_{A1}(k_{ci}^{x}r)Z_{B1}(k_{cm}^{y}r)rdr \\
&= B_0\left[e^{\gamma_{B0}d}+\Gamma_{B0}e^{-\gamma_{B0}d}\right]\sum_{x=x_1}^{x_t}\varepsilon^x\int_{R_{1x}}^{R_{2x}}Z_{A1}(k_{ci}^{x}r)dr
\end{aligned}
$$

$$
\begin{aligned}
&+\sum_{m=1}^{\infty} B_m \left[e^{\gamma_m d}+\Gamma_{Bm}e^{-\gamma_m d}\right] \\
&\times \sum_{x=x_1}^{x_t} \varepsilon^x \int_{R_{1x}}^{R_{2x}} Z_{A1}(k_{ci}^x r) Z_{B1}(k_{cm}^y r) r dr \\
= \;& B_0 \left[e^{\gamma_{B0} d}+\Gamma_{B0}e^{-\gamma_{B0} d}\right] \\
&\times \sum_{x=x_1}^{x_t} \varepsilon^x \left[-Z_{A0}(k_{ci}^x R_{2x})+Z_{A0}(k_{ci}^x R_{1x})\right]/k_{ci}^x \\
&+\sum_{m=1}^{\infty} B_m \left[e^{\gamma_m d}+\Gamma_{Bm}e^{-\gamma_m d}\right] \\
&\times \sum_{xy=xy_1}^{xy_t} \varepsilon_A^{xy} \left[f_{AiBm}^{xy}(R_{2xy})-f_{AiBm}^{xy}(R_{1xy})\right], \qquad (46)
\end{aligned}
$$

where $t_A$ is the total layer number of filling material in Section A, $x_1$ and $x_t$ are respectively the first layer number and the last layer number in the range $\max(R_{1a}, R_{1b})$ to $\min(R_{2a}, R_{2b})$ in Section A, $y_1$ and $y_t$ are respectively the first layer number and the last layer number in the range $\max(R_{1a}, R_{1b})$ to $\min(R_{2a}, R_{2b})$ in Section B, $xy_1$ and $xy_t$ are respectively the first and the last layer number in the range from $\max(R_{1A}, R_{1B})$ to $\min(R_{2A}, R_{2B})$ on the interface between Section A and Section B, $R_{2x}$ and $R_{1x}$ are respectively the outer and the inner radius of the $x$th layer in Section A, $R_{2y}$ and $R_{1y}$ are respectively the outer and the inner radius of the $y$th layer in Section B, $R_{2xy}$ and $R_{1xy}$ are respectively the outer and the inner radius of the $xy$th layer on the interface between Section A and Section B, $\varepsilon_A^{xy}$ is the Section A's permittivity of the $xy$th discontinuity layer on the interface, and

$$
f_{Ai}^x(r) = \frac{r^2}{2}\left[Z_{A1}^2(k_{ci}^x r)-Z_{A0}(k_{ci}^x r)Z_{A2}(k_{ci}^x r)\right], \qquad (47)
$$

$$
\begin{aligned}
f_{AiBm}^{xy}(r) = \;& \int Z_{A1}(k_{ci}^x r) Z_{B1}(k_{cm}^y r) r dr = \frac{r}{(k_{ci}^x)^2-(k_{cm}^y)^2} \\
&\times \left[k_{cm}^y Z_{B0}(k_{cm}^y r) Z_{A1}(k_{ci}^x r)-k_{ci}^x Z_{A0}(k_{ci}^x r) Z_{B1}(k_{cm}^y r)\right]. \qquad (48)
\end{aligned}
$$

The second step is to perform the following integral at both sides of (42):

$$
\int_{R_{1b}}^{R_{2b}} E_{Brm} H_{B\phi} 2\pi r dr. \qquad (49)
$$

From the integral above, the following equations can be obtained:

$$\begin{aligned}
& -\sqrt{\frac{\varepsilon_B}{\mu_B}}B_0\left[e^{\gamma_{B0}d}-\Gamma_{B0}e^{-\gamma_{B0}d}\right]\int_{R_{1a}}^{R_{2a}}\frac{1}{r}dr \\
= & -\sqrt{\frac{\varepsilon_B}{\mu_B}}B_0\left[e^{\gamma_{B0}d}-\Gamma_{B0}e^{-\gamma_{B0}d}\right]\ln\frac{R_{2b}}{R_{1b}} \\
= & -\sqrt{\frac{\varepsilon_A}{\mu_A}}A_0\left(1-\Gamma_{A0}\right)\int_{\max(R_{1a},R_{1b})}^{\min(R_{2a},R_{2b})}\frac{1}{r}dr \\
& +\sum_{i=1}^{\infty}A_i(1-\Gamma_{Ai})\frac{-j\omega}{\gamma_i}\int_{\max(R_{1a},R_{1b})}^{\min(R_{2a},R_{2b})}\varepsilon^x Z_{A1}(k_{ci}^x r)dr \\
= & -\sqrt{\frac{\varepsilon_A}{\mu_A}}A_0\left(1-\Gamma_{A0}\right)\ln\frac{\min(R_{2a},R_{2b})}{\max(R_{1a},R_{1b})}+\sum_{i=1}^{\infty}A_i(1-\Gamma_{Ai})\frac{-j\omega}{\gamma_i} \\
& \times\sum_{x=x_1}^{x_t}\varepsilon^x\left[-Z_{A0}(k_{ci}^x R_{2x})+Z_{A0}(k_{ci}^x R_{1x})\right]/k_{ci}^x, \qquad (50)
\end{aligned}$$

$$\begin{aligned}
& B_m\left[e^{\gamma_m d}+\Gamma_{Bm}e^{-\gamma_m d}\right]\int_{R_{1b}}^{R_{2b}}\frac{-j\omega\varepsilon^y}{\gamma_m}Z_{B1}^2(k_{cm}^y r)rdr \\
= & B_m\left[e^{\gamma_m d}+\Gamma_{Bm}e^{-\gamma_m d}\right]\frac{-j\omega}{\gamma_m}\sum_{y=1}^{t_B}\varepsilon^y\left[f_{Bm}^y(R_{2y})-f_{Bm}^y(R_{1y})\right] \\
= & -\sqrt{\frac{\varepsilon_A}{\mu_A}}A_0\left(1-\Gamma_{A0}\right)\int_{\max(R_{1a},R_{1b})}^{\min(R_{2a},R_{2b})}Z_{B1}(k_{cm}^y r)dr \\
& +\sum_{i=1}^{\infty}A_i(1-\Gamma_{Ai})\int_{\max(R_{1a},R_{1b})}^{\min(R_{2a},R_{2b})}\frac{-j\omega\varepsilon^x}{\gamma_i}Z_{A1}(k_{ci}^x r)Z_{B1}(k_{cm}^y r)rdr \\
= & -\sqrt{\frac{\varepsilon_A}{\mu_A}}A_0\left(1-\Gamma_{A0}\right)\sum_{y=y_1}^{y_t}\int_{R_{2y}}^{R_{1y}}Z_{B1}(k_{cm}^y r)dr \\
& +\sum_{i=1}^{\infty}A_i(1-\Gamma_{Ai})\frac{-j\omega}{\gamma_i}\sum_{x=x_1}^{x_t}\varepsilon^x\int_{R_{1x}}^{R_{2x}}Z_{A1}(k_{ci}^x r)Z_{B1}(k_{cm}^y r)rdr \\
= & -\sqrt{\frac{\varepsilon_A}{\mu_A}}A_0\left(1-\Gamma_{A0}\right)\sum_{y=y_1}^{y_t}\left[-Z_{B0}(k_{cm}^y R_{2y})+Z_{B0}(k_{cm}^y R_{1y})\right]/k_{cm}^y \\
& +\sum_{i=1}^{\infty}A_i(1-\Gamma_{Ai})\frac{-j\omega}{\gamma_i}\sum_{xy=xy_1}^{xy_t}\varepsilon_A^{xy}\left[f_{AiBm}^{xy}(R_{2xy})-f_{AiBm}xy(R_{1xy})\right], \\
& \qquad (51)
\end{aligned}$$

where $t_B$ is the total layer number of the filling material in Section B,

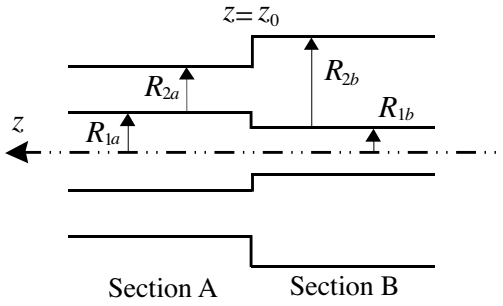


**Figure 4.** Illustration of mode matching at certain filling material layers.

and

$$f_{Bm}^{y}(r) = \frac{r^2}{2}\left[Z_{B1}^2(k_{cm}^{y}r) - Z_{B0}(k_{cm}^{y}r)Z_{B2}(k_{cm}^{y}r)\right]. \tag{52}$$

The two-step mode matching procedure in (44) and (49) is valid as long as the cross section of Section A is not larger than that of Section B. In the case where the cross section of Section B is larger than that of Section A, as is showed in Fig. 4, the mode matching procedure as follows should be used instead of (44) and (49) to ensure correctly enforcing the traverse electric field continuity on the interface between Section A and Section B [29]:

$$\int_{R_{1b}}^{R_{2b}} E_{Br}H_{B\phi m}2\pi r dr, \tag{53}$$

$$\int_{R_{1a}}^{R_{2a}} E_{Ari}H_{A\phi}2\pi r dr. \tag{54}$$

Based on (53) and (54), the following equations can be obtained:

$$B_0\left[e^{\gamma_{B0}d} + \Gamma_{B0}e^{-\gamma_{B0}d}\right]\ln\frac{R_{2b}}{R_{1b}} = A_0(1+\Gamma_{A0})\ln\frac{\min(R_{2a},R_{2b})}{\max(R_{1a},R_{1b})} + \sum_{i=1}^{\infty}A_i(1+\Gamma_{Ai})\sum_{x=x_1}^{x_t}\left[-Z_{A0}(k_{ci}^{x}R_{2x}) + Z_{A0}(k_{ci}^{x}R_{1x})\right]/k_{ci}^{x}, \tag{55}$$

$$B_m\left[e^{\gamma_m d} + \Gamma_{Bm}e^{-\gamma_m d}\right]\sum_{y=1}^{t_B}\varepsilon^{y}\left[f_{Bm}^{y}(R_{2y}) - f_{Bm}^{y}(R_{1y})\right] = A_0(1+\Gamma_{A0})\sum_{y=y_1}^{y_t}\varepsilon^{y}\left[-Z_{B0}(k_{cm}^{y}R_{2y}) + Z_{B0}(k_{cm}yR_{1y})\right]/k_{cm}^{y}$$

$$+\sum_{i=1}^{\infty} A_i(1+\Gamma_{Ai}) \sum_{xy=xy_1}^{xy_t} \varepsilon_B^{xy}[f_{AiBm}^{xy}(R_{2xy}) - f_{AiBm}^{xy}(R_{1xy})], \quad (56)$$

$$-\sqrt{\frac{\varepsilon_A}{\mu_A}} A_0(1-\Gamma_{A0}) \ln \frac{R_{2a}}{R_{1a}}$$
$$= -\sqrt{\frac{\varepsilon_B}{\mu_B}} B_0 \left(e^{\gamma_{B0}d} - \Gamma_{B0} e^{-\gamma_{B0}d}\right) \ln \frac{\min(R_{2a}, R_{2b})}{\max(R_{1a}, R_{1b})}$$
$$+\sum_{m=1}^{\infty} \frac{-j\omega}{\gamma_m} B_m \left(e^{\gamma_m d} - \Gamma_{Bm} e^{-\gamma_m d}\right)$$
$$\times \sum_{y=y_1}^{y_t} \varepsilon^y \left[-Z_{B0}(k_{cm}^y R_{2y}) + Z_{B0}(k_{cm}^y R_{1y})\right] / k_{cm}^y, \quad (57)$$

$$\frac{-j\omega}{\gamma_i} A_i(1-\Gamma_{Ai}) \sum_{x=1}^{t_A} \varepsilon^x \left[f_{Ai}^x(R_{2x}) - f_{Ai}^x(R_{1x})\right]$$
$$= -\sqrt{\frac{\varepsilon_B}{\mu_B}} B_0 \left[e^{\gamma_{B0}d} - \Gamma_{B0} e^{-\gamma_{B0}d}\right]$$
$$\times \sum_{x=x_1}^{x_t} \left[-Z_{A0}(k_{ci}^x R_{2x}) + Z_{A0}(k_{ci}^x R_{1x})\right] / k_{ci}^x$$
$$\sum_{m=1}^{\infty} \frac{-j\omega}{\gamma_m} B_m \left[e^{\gamma_m d} - \Gamma_{Bm} e^{-\gamma_m d}\right]$$
$$\times \sum_{xy=xy_1}^{xy_t} \varepsilon_B^{xy}[f_{AiBm}^{xy}(R_{2xy}) - f_{AiBm}^{xy}(R_{1xy})], \quad (58)$$

Where $\varepsilon_B^{xy}$ is the Section B's permittivity of the $xy$th discontinuity layer on the interface.

Suppose that the total number of sections in the structure is $sn$, and the number of modes retained for the Section $i$ is $m_i$. Then the total number of discontinuities is $sn$-1. After the two steps of mode matching procedure above are performed at each discontinuity interface, a set of simultaneous equations which contain the unknown variables, $\ldots, A_i, A_i\Gamma_{Ai}, \ldots, B_m, B_m\Gamma_{Bm}, \ldots$, can be obtained. Apparently, the number of unknown variables is $2 \times (m_1 + m_2 + \ldots + m_{sn})$, and the number of equations is $m_1 + 2 \times (m_2 + \ldots + m_{sn-1}) + m_{sn}$. The equations can not be solved until the termination conditions for the first and the last sections are taken into account.

For the termination condition of the first section shown in Fig. 5(a), it is reasonable to assume that all the modes of wave will only traveling in the $z$ direction in the first section, except for the incident

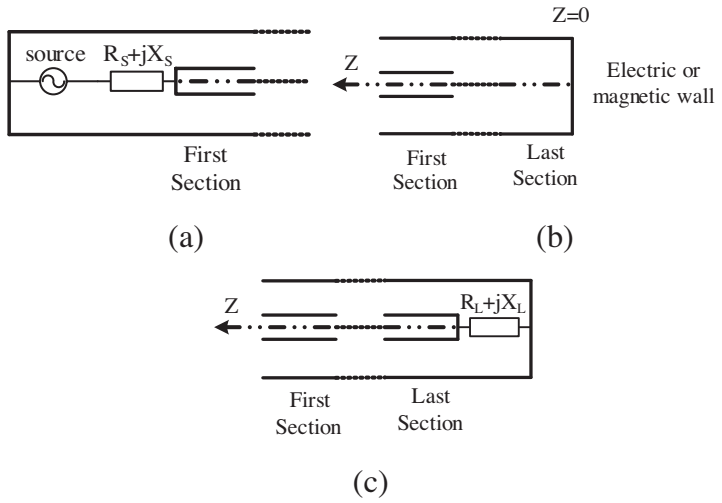


**Figure 5.** Termination conditions of the axisymmetrical structure. (a) First section is connected to source with the source impedance $R_S + jX_S$. (b) Last section is terminated by electric or magnetic wall. (c) Last section is terminated by lumped impedance $R_L + jX_L$.

TEM wave. Actually, it is often the case that a coaxial waveguide used as sample holders is designed only for the propagation of the TEM wave, and all the high order modes will attenuate to zero very fast far before they reach the source impedance. Furthermore, in the general cases, the characteristic impedance of the first section of the coaxial structure is designed to be equal to the source impedance. The reflected TEM wave from the first discontinuity will not be reflected again when they reach the source impedance. Thus, from (32) and (34), the transverse electromagnetic field components in the first section can be written as follows:

$$E_{Ar} = \frac{A_0}{r}\left[e^{\gamma_{A0}(z-z_0)} + \Gamma_{A0}e^{-\gamma_{A0}(z-z_0)}\right] + \sum_{i=1}^{\infty} A_i Z_{A1}(k_{ci}^x r)\Gamma_{Ai}e^{-\gamma_i(z-z_0)}, \qquad R_{1a} < r < R_{2a}, \quad (59)$$

$$H_{A\phi} = -\sqrt{\frac{\varepsilon_A}{\mu_A}}\frac{A_0}{r}\left[e^{\gamma_{A0}(z-z_0)} - \Gamma_{A0}e^{-\gamma_{A0}(z-z_0)}\right] + \sum_{i=1}^{\infty}\frac{j\omega\varepsilon^x}{\gamma_i}A_i Z_{A1}(k_{ci}^x r)\Gamma_{Ai}e^{-\gamma_i(z-z_0)}, \quad R_{1a}<r<R_{2a}. \quad (60)$$

It can be seen from the two equations above that the number of unknown variables is reduced by $m_1 - 1$. The number of unknown variables can be further reduced by 1 since the amplitude of the incident wave is assumed known.

When the last section is terminated by an electric wall as in Fig. 5(b), due to the electric field boundary condition at this plane, $\Gamma_{Bm}$ is $-1$. When a magnetic wall is used to terminate the last section, $\Gamma_{Bm}$ is 1. For the termination condition in Fig. 5(c), the last section is terminated by lumped impedance. Again, in the usual case, the termination impedance is equal to the characteristic impedance of the last section of the coaxial waveguide. And the high order modes will go to zero quickly. Under these assumptions, all the waves will travel only toward the $-z$ direction, and the reflection coefficients $\Gamma_{Bm}$ are all zeros.

Apparently, the termination conditions of the last section reduce the number of unknown variables by $m_{sn}$.

Up to now, with the termination conditions taken into account, the number of unknown variables is equal to the number of equations. The simultaneous equations can be solved. The distribution of the electromagnetic field in the structure and the $s$ parameters can be readily obtained.

## 5. NUMERICAL RESULTS

In this section, we apply the method above to calculate the $s$ parameters of three kinds of coaxial discontinuity structures in Fig. 6 which are used in the complex permittivity and permeability measurement [1, 2, 4, 6]. The diameter $d$ of the inner conductor of the coaxial structures is 3.04 mm. The inner diameter $D$ of the outer conductor is 7 mm. For the structures in Fig. 6(a)–(b), the material under test is assumed to be Mn-Zn ferrite. The height of the material under test in Fig. 6(a) and Fig. 6(b) are 1 mm and 2 mm respectively. The permeability and the permittivity of the Mn-Zn ferrite are given below [26], both of which are frequency dependent:

$$\varepsilon = \varepsilon' - j\varepsilon'', \tag{61}$$

$$\varepsilon' = \frac{\varepsilon_0\varepsilon_r g^2}{\omega^2(\varepsilon_0\varepsilon_r)^2 + g^2}, \tag{62}$$

$$\varepsilon'' = \frac{\omega(\varepsilon_0\varepsilon_r)^2 g}{\omega^2(\varepsilon_0\varepsilon_r)^2 + g^2}, \tag{63}$$

$$\mu = \mu' - j\mu'', \tag{64}$$

$$\mu' = \frac{\mu_0\mu_r\lambda^2}{\omega^2(\mu_0\mu_r)^2+\lambda^2}, \tag{65}$$

$$\mu'' = \frac{\omega(\mu_0\mu_r)^2\lambda^2}{\omega^2(\mu_0\mu_r)^2+\lambda^2}, \tag{66}$$

$$\lambda = \frac{\lambda_h\lambda_f}{\lambda_h+\lambda_f}, \tag{67}$$

$$\lambda_h = \lambda_{h0}\frac{\omega}{\omega_0}, \tag{68}$$

where $g = 10\,\mathrm{s/m}$, $\varepsilon_r = 10^5$, $\mu_r = 3080$, $\lambda_f = 57\times10^3\,\Omega/\mathrm{m}$, $\lambda_{h0} = 615\,\Omega/\mathrm{m}$, and $\omega_0 = 2\pi\times1000\,\mathrm{rad/s}$.

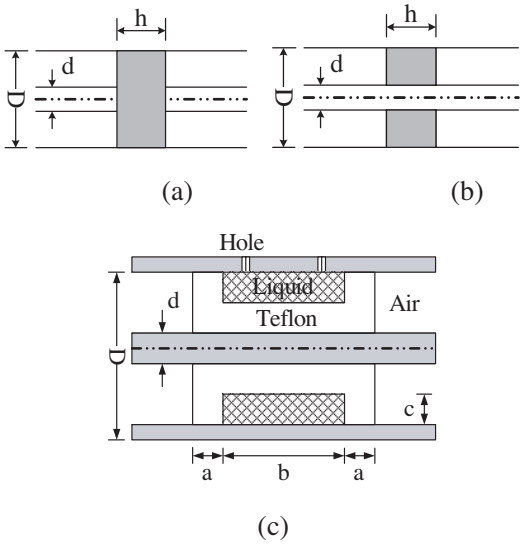


**Figure 6.** Coaxial discontinuity structures used for material characterization.

The structure in Fig. 6(c) is presented in [6] for material characterization of liquid and powder. It is assumed here the Teflon container ($\varepsilon' = 2.31\varepsilon_0$, $\tan\delta = 1\times10^{-4}$) is used to hold a liquid sample which is nonmagnetic and has unvaried complex permittivity as $\varepsilon = (30.89 - 7.13i)\varepsilon_0$ in the considered frequency range 500 kHz–1 GHz. The other dimension parameters of the structure are $a = 2\,\mathrm{mm}$, $b = 10\,\mathrm{mm}$, and $c = 1\,\mathrm{mm}$.

Before the mode matching method is used to solve the s parameters, the propagation constants of all the sections have to be solved first.

A numerical routine is used to find the roots of (2). At the same time, the propagation constants are solved by using the one-dimensional finite difference method in Section 2. The results of these two methods are shown in Table 1. It can be seen that the two sets of results are in excellent agreement.

**Table 1.** Comparison of propagation constants of symmetrical TM modes in air filled coaxial waveguide ($f = 1\,\text{MHz}$, $\Delta r = 1 \times 10^{-5}\,\text{m}$).

| Mode | Roots of (2) | One-dimension finite difference method |
|---|---|---|
| $TM_{01}$ | 1573.26 | 1573.25 |
| $TM_{02}$ | 3166.14 | 3166.01 |
| $TM_{03}$ | 4755.12 | 4754.68 |
| $TM_{04}$ | 6342.98 | 6341.92 |
| $TM_{05}$ | 7930.37 | 7928.30 |
| $TM_{06}$ | 9517.52 | 9513.93 |

The roots of (6) found by a numerical routine and the propagation constants solved by the one-dimensional finite difference method are shown in Table 2. Again, good agreement between the two sets of results is observed.

**Table 2.** Comparison of propagation constants of symmetrical TM modes in material under test filling circular waveguide ($f = 1\,\text{MHz}$, $\Delta r = 1 \times 10^{-5}\,\text{m}$).

| Mode | Roots of (6) | One-dimension finite difference method |
|---|---|---|
| $TM_{01}$ | 661.96 + 118.51i | 661.96 + 118.51i |
| $TM_{02}$ | 1562.70+50.20i | 1562.68+50.20i |
| $TM_{03}$ | 2462.98+31.85i | 2462.92+31.85i |
| $TM_{04}$ | 3361.97+23.33i | 3361.81+23.34i |
| $TM_{05}$ | 4260.39+18.41i | 4260.07+18.41i |
| $TM_{06}$ | 5158.54+15.21i | 5157.96+15.21i |

For the section filled by the material under test in Fig. 6(b), we assume that the coaxial waveguide is not fully filled by the material under test. The widths of both the inner air gap and the outer air gap are 0.1 mm. The propagation constants of the quasi-TEM mode and the symmetrical TM modes can be solved by the field matching technique given in [22]. Based on the continuity conditions of the transverse field components at the discontinuity interface, a matrix $[A(\gamma)]$ is formed in [22]. The elements of the matrix contain the propagation constants $\gamma$. The method of solving the propagation constants is to try values of $\gamma$ and test for the determinant of the matrix to be zero. But the actual implementation of searching is a difficult task because of the fact that $\det([A(\gamma)])$ is a rapidly changing function with $\gamma$, containing not only poles and zeros in close neighborhood but also extremely steep gradients. A method to circumvent this problem is presented in [27] where the singular-value decomposition of the matrix $[A(\gamma)]$ is used instead of $\det([A(\gamma)])$.

The propagation constants solved by the one-dimensional finite difference method and the field matching technique with the singular-value decomposition searching technique are shown in Table 3. The two sets of results are in excellent agreement. Since the propagation constants are not real or pure imaginary, it takes time to search for the propagation constants in the complex plane using the field matching technique. It is found that even with the singular-value decomposition searching technique, it is hard to find some high order modes by using the field matching technique due to the fact that the sharpness of a minimum in the smallest singular value increases as its location approaches a pole of the determinant [28]. Therefore, the numerical search algorithm has to operate at very small step widths. The minimum singular values around some propagation constants are shown in Fig. 7. Given that the searching step widths in the real and the imaginary axes are 0.25 when the field matching technique is used to roughly search the propagation constants, the required number of searching for all the propagation constants in Table 3 will be at least $7066 \times 44 \times 16 = 4974464$. The average time needed for each searching operation, i.e., construction and singular-value decomposition of the matrix $[A(\gamma)]$, is approximately 0.0025 seconds when a P4 3.4 GHz PC is used. Thus the time needed to roughly search the propagation constants can be estimated to be more than 3 hours. After the approximate values of the propagation constants are obtained, the simplex method can be used to refine the results. For the one-dimensional finite difference method, the time needed to solve all the propagation constants is less than 1 second when the same PC is used. Apparently, the one-dimensional finite difference method is much more

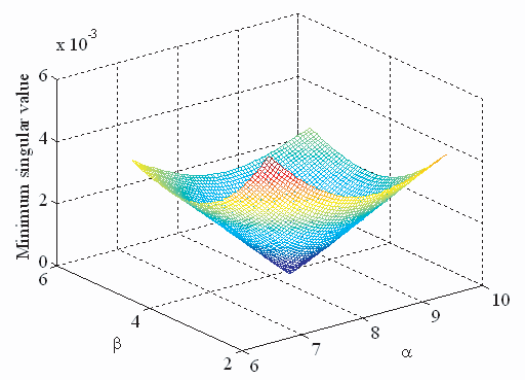


(a)

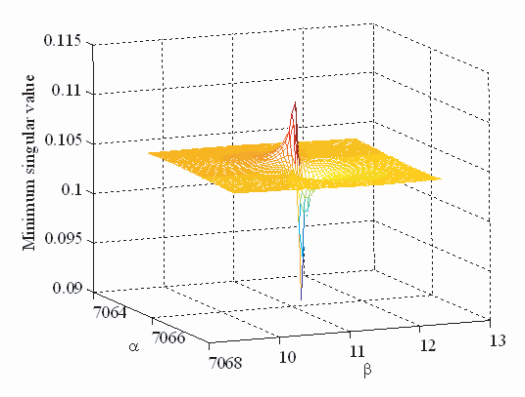


(b)

**Figure 7.** Minimum singular values of the matrix used to find $\gamma$ in Table 3. (a) around $\gamma$ of $TM_{01}$. (b) around $\gamma$ of $TM_{05}$.

efficient.

For the multi-layered structures, after the propagation constants are solved, the modal field patterns can be readily obtained by using the least square method as mentioned in Section 3. As one example, for the mode $TM_{03}$ in Table 3, the eigenvectors of (20) and the least square fitting results of (29) are shown in Fig. 8(a). The $E_r$ field distribution by (28) is shown in Fig. 8(b). The $E_z$ field distribution by (25) is shown in Fig. 8(c).

For the structure in Fig. 6(a), the $s$ parameters are respectively calculated by using the method in the paper, the method in [4], and a two-dimensional frequency domain finite difference method which is

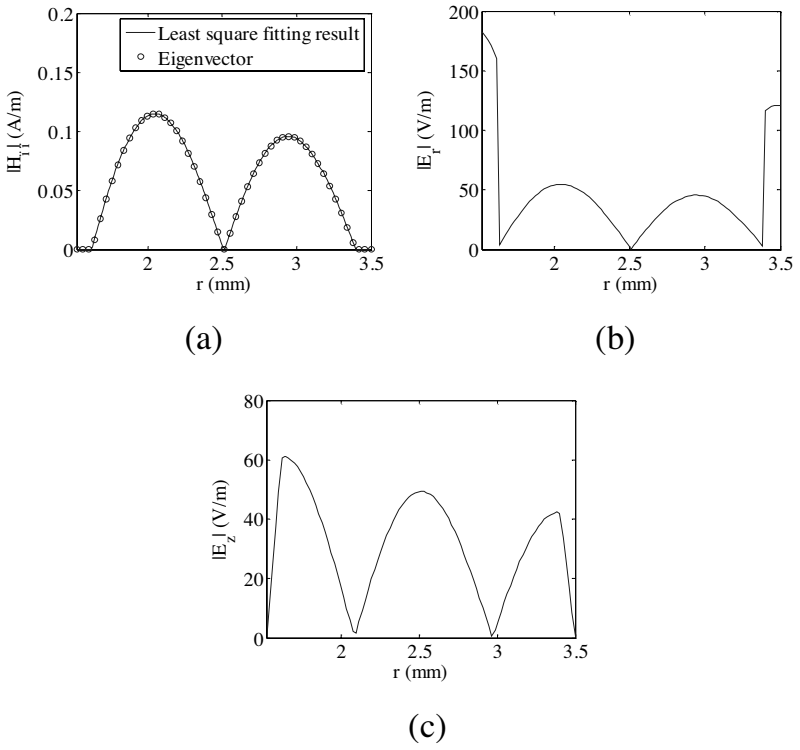


**Figure 8.** Modal field patterns determined by least square method for $TM_{03}$ in Table 3. (a) $H_\phi$ field distribution. (b) $E_r$ field distribution. (c) $E_z$ field distribution.

**Table 3.** Comparison of propagation constants of Quasi-TEM mode and symmetrical TM modes in material under test partly filled coaxial waveguide ($f = 1\,\text{MHz}$, $\Delta r = 1 \times 10^{-5}\,\text{m}$).

| Mode | Field matching technique | One-dimension finite difference method |
|---|---|---|
| Quasi-TEM | 0.7460+3.0601i | 0.7460+3.0601i |
| $TM_{01}$ | 8.2338+3.8909i | 8.2338+3.8909i |
| $TM_{02}$ | 1787.27+43.92i | 1787.25+43.92i |
| $TM_{03}$ | 3541.98+22.16i | 3541.80+22.17i |
| $TM_{04}$ | 5303.03+14.80i | 5302.42+14.81i |
| $TM_{05}$ | 7065.96+11.11i | 7064.50+11.11i |

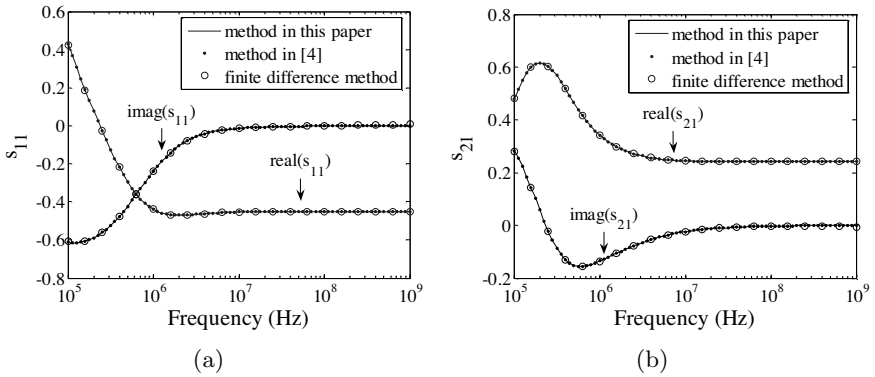


**Figure 9.** Result comparison of the method in this paper, the method in [4] and the two-dimension frequency domain finite difference method for the structure in Fig. 6(a).

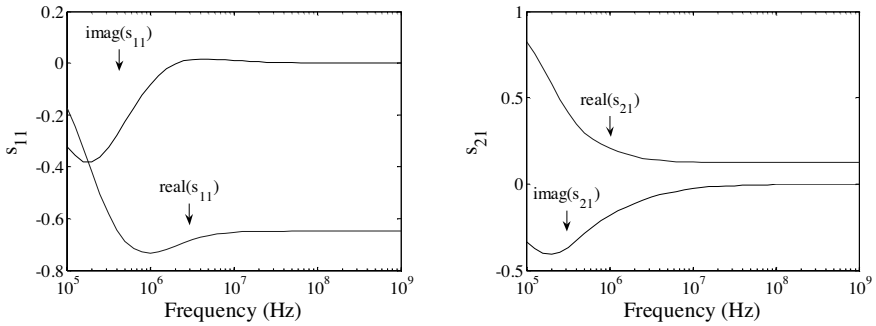


**Figure 10.** Result of the analytical method for the first case of structure in Fig. 6(b).

based on the two-dimensional FDTD method [9, 10]. The results are shown in Fig. 9.

For the structure in Fig. 6(b), in the first case, we assume that the material under test perfectly fills up the cross section of the coaxial sample holder. In this case, it can be predicted that only TEM mode exists in the whole structure. The s parameters can be easily calculated by the analytical method [1, 2]. Results of the analytical method are shown in Fig. 10. In the second case, we assume that there is a 0.1 mm air gap between the material under test and the inner conductor of the coaxial holder. Results of the method in this paper and the two-dimensional frequency domain finite difference method are shown in

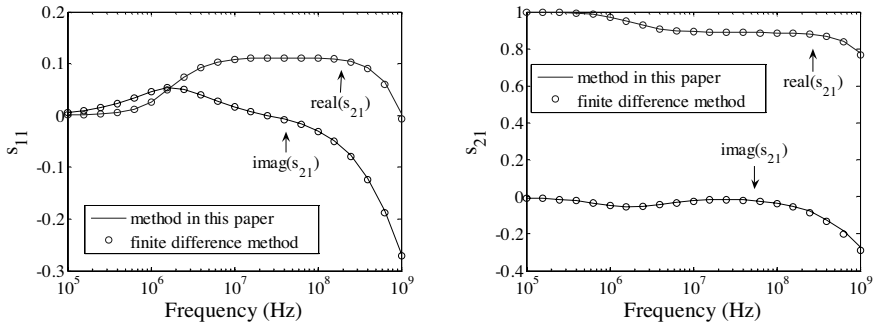


**Figure 11.** Result comparison of the method in this paper and the two-dimension frequency domain finite difference method for the second case of structure in Fig. 6(b).

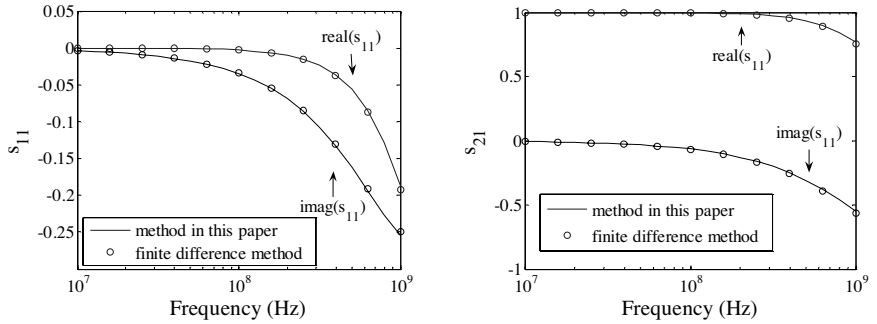


**Figure 12.** Result comparison of the method in this paper and the two-dimension frequency domain finite difference method for the structure in Fig. 6(c).

Fig. 11. It is interesting to note that only a small air gap between the material under test and the conductor of the coaxial holder makes the $s$ parameters totally different.

For the structure in Fig. 6(c), results of the method in this paper and the two-dimensional frequency domain finite difference method are shown in Fig. 12.

In these numerical examples, good agreement between the results of the method in this paper and those of other methods in the references is observed.

## 6. CONCLUSION

In this paper, the mode matching method has been applied to the analysis of coaxial discontinuity structures commonly used in the permeability and/or permittivity measurement. The propagation constants of the coaxial waveguides and the circular waveguides filled with multi-layered materials are efficiently solved by a one-dimensional frequency domain finite difference method. The numerical results of the approach in this paper are in good agreement with those of other methods in references. The general solution provided by the approach in this paper makes the analysis of this kind of structures very convenient.

## REFERENCES

1. Nicolson, A. M. and G. F. Ross, "Measurement of the intrinsic properties of materials by time-domain techniques," *IEEE Trans. Instrum. Meas.,* Vol. IM-19, 377–382, Nov. 1970.
2. Weir, W. B., "Automatic measurement of complex dielectric constant and permeability at microwave frequencies," *Proc. IEEE,* Vol. 62, No. 1, 33–36, Jan. 1974.
3. Belhadj-Tahar, N.-E. and A. Fourrier-Lamer, "Broad-band analysis of a coaxial discontinuity used for dielectric measurements," *IEEE Trans. Microwave Theory Tech.,* Vol. 34, No. 3, 346–350, Mar. 1986.
4. Belhadj-Tahar, N.-E., A. Fourrier-Lamer, and H. de Chanterac, "Broad-band simultaneous measurement of complex permittivity and permeability using a coaxial discontinuity," *IEEE Trans. Microwave Theory Tech.,* Vol. 38, No. 1, 1–7, Jan. 1990.
5. Obrzut, J. and A. Anopchenko, "Input impedance of a coaxial line terminated with a complex gap capacitance — numerical and experimental analysis," *IEEE Trans. Instrum. Meas.,* Vol. 53, No. 4, 1197–1201, Aug. 2004.
6. Huang, J., K. Wu, P. Morin, and C. Akyel, "Characterization of highly dispersive materials using composite coaxial cells: electromagnetic analysis and wideband measurement," *IEEE Trans. Microwave Theory Tech.,* Vol. 44, No. 5, 770–777, May 1996.
7. Wexler, A., "Solution of waveguide discontinuities by modal analysis," *IEEE Trans. Microwave Theory Tech.,* Vol. 15, No. 9, 508–517, Sep. 1967.
8. Eom, H. J., Y. C. Noh, and J. K. Park, "Scattering analysis of a

coaxial line terminated by a gap," *IEEE Microwave and Guided Wave Letters,* Vol. 8, No. 6, 218–219, June 1998.

9. Davidovich, M. V., "Full-wave analysis of coaxial mounting structure," *IEEE Trans. Microwave Theory Tech.,* Vol. 47, No. 3, 265–270, Mar. 1999.
10. Wilkins, G. M., J.-F. Lee, and R. Mittra, "Numerical modeling of axisymmetric coaxial waveguide discontinuities," *IEEE Trans. Microwave Theory Tech.,* Vol. 39, No. 8, 1323–1328, Aug. 1991.
11. Chen, Y., R. Mittra, and P. Harms, "Finite-difference time-domain algorithm for solving Maxwell's equations in rotationally symmetric geometries," *IEEE Trans. Microwave Theory Tech.,* Vol. 44, No. 6, 832–839, June 1996.
12. Yu, W., R. Mittra, and S. Dey, "Application of the nonuniform FDTD technique to analysis of coaxial discontinuity structures," *IEEE Trans. Microwave Theory Tech.,* Vol. 49, No. 1, 207–209, Jan. 2001.
13. Holland, R., "Finite difference solutions of Maxwell's equations in generalized nonorthogonal coordinates," *IEEE Trans. Nuc. Sci.*, Vol. NS-30, No. 6, 4589–4591, Dec. 1983.
14. Fusco, M., "FDTD algorithm in curvilinear coordinates," *IEEE Trans on Antennas and Propagation*, Vol. 38, No. 1, 76–89, Jan. 1990.
15. Zhao, Y. J., K. L. Wu, and K. K. M. Cheng, "A compact 2-D full-wave finite-difference frequency-domain method for general guided wave structures," *IEEE Trans. Microwave Theory Tech.,* Vol. 50, No. 7, 1844–1848, July 2002.
16. Pereda, J. A., A. Vegas, and A. Prieto, "An improved compact 2D fullwave FDFD method for general guided wave structures," *Microwave and Optical Technology Letters,* Vol. 38, No. 4, 331–335, Aug. 2003.
17. Li, L. Y. and J. F. Mao, "An improved compact 2-D finite-difference frequency-domain method for guided wave structures," *IEEE Microwave and Wireless Components Letters,* Vol. 13, No. 12, 520–522, Dec. 2003.
18. Wang, B. Z., X. H. Wang, and W. Shao, "2D full-wave finite-difference frequency-domain method for lossy metal waveguide," *Microwave and Optical Technology Letters,* Vol. 42, No. 2, 158–161, July 2004.
19. Haffa, S., D. Hollmann, and W. Wiesbeck, "The finite difference method for S-parameter calculation of arbitrary three-dimensional structures," *IEEE Trans. Microwave Theory Tech.,* Vol. 40, No. 8,

1602–1610, Aug. 1992.

20. Bardi, I. and O. Biro, "An efficient finite-element formulation without spurious modes for anisotropic waveguides," *IEEE Trans. Microwave Theory Tech.,* Vol. 39, No. 7, 1133–1139, July 1991.
21. Angkaew, T., M. Matsuhara, and N. Kumagai, "Finite-element analysis of waveguide modes: a novel approach that eliminates spurious modes," *IEEE Trans. Microwave Theory Tech.,* Vol. 35, No. 2, 117–123, Feb. 1987.
22. Williams, D. J., C. J. Railton, and D. J. Edwards, "A mathematical model of concentrically loaded coaxial structures and its EMC applications," *7th International Conference on Electromagnetic Compatibility,* 91–98, Aug. 1990.
23. Marcuvitz, N., *Waveguide Handbook,* Peter Peregrinus Ltd., London, 1986.
24. Kong, J. A., *Electromagnetic Wave Theory,* 2nd ed., Wiley, New York, 1990.
25. Andrews, L. C., *Special Functions for Engineers and Applied Mathematicians,* McGraw-Hill, New York, 1962.
26. Zhang, D. M. and C. F. Foo, "Theoretical analysis of the electrical and magnetic field distributions in a toroidal core with circular cross section," *IEEE T MAGN,* Part 2, Vol. 35, No. 3, 1924–1931, May 1999.
27. Labay, V. and J. Bornemann, "Matrix singular value decomposition for pole-free solutions of homogeneous matrix equations as applied to numerical modeling methods," *IEEE Microwave and Guided Wave Letters,* Vol. 2, No. 2, 49–51, Feb. 1992.
28. Amari, S. and J. Bornemann, "A pole-free modal field-matching technique for eigenvalue problems in electromagnetics," *IEEE Trans. Microwave Theory Tech.,* Vol. 45, No. 9, 1649–1653, Sep. 1997.
29. Eleftheriades, G. V., A. S. Omar, L. P. B. Katehi, and G. M. Rebeiz, "Some important properties of waveguide junction generalized scattering matrices in the context of the mode matching technique," *IEEE Trans. Microwave Theory Tech.*, Vol. 42, No. 10, 1896–1903, Oct. 1994.